frontiers

Isometric Torque Values About Robotic Knee Using Braided Pneumatic Actuators

Ben Bolen [1,*], **Lindie Burgess** [1], **Connor Morrow** [1], **Lawrence Pang** [1], **Cody Scharzenberger** [1], **and Alex Hunt** [1]

[1] *Agile and Adaptive Robotics Laboratory, Portland State University, Department of Mechanical and Materials Engineering, Portland, OR, USA*

Correspondence*:
Ben Bolen
Portland State University, Department of Mechanical and Materials Engineering, PO Box 751, Portland, OR, 97207-0751, USA
bbolen83@gmail.com

ABSTRACT

Artificial muscles such as braided pnuematic actuators (BPAs) offer many advantages for robotic systems, including high durability and and strength-to-weight ratios. However, their use in robotic systems are still extremely limited, in part due to their poor characterization, especially with regard to their force and length capabilities. In this work, test setups are created to compare forces and torques produced by Festo fluidic braided pneumatic actuators (BPAs) with leading models. The muscle force setup consists of linear force recordings while the robotic system consists of a lower limb model of a bipedal humanoid robot that was designed to achieve biomimetic ranges of motion and isometric torque values. Predicted torque values based on developed models are compared with recorded torque data to determine the major sources of error in current modeling tools. Our analysis of the data has resulted in the development of new equations to calculate force as functions of pressure and strain for muscles with diameters of 10 mm and 20 mm. We have also developed a novel equation for maximum force in the 10 mm diameter BPA as a function of resting length. The improved force calculations reduced the difference between measured and calculated torque in the robot, but are unable to explain all the discrepancies. An improved model is better able to match the experimental data by including a series spring element in the BPA model. Finally, we show that a properly sized BPA can be used to meet or exceed human isometric knee torque values. This work demonstrates a greatly improved model that is better able to predict joint torques produced by Festo BPAs on biomimetic designs. This will lead to faster design processes and the development of biomimetic robots that are able to more accurately reproduce the range of motion and isometric torque profiles that exist in the animals they are mimicking.

Keywords: BPA, Biomimetic, Function Fit, PAM, Artificial Muscle, Bioinspired, Bipedal Robot, Isometric Knee Torque

1 INTRODUCTION

Both academic researchers and the general public are keenly interested in biomimetic robots due to their many applications. In the discipline of biomimetic robotics, high fidelity robots can help improve our understanding of both biomechanics and the underlying neuromechanical systems that control them (Shin

et al., 2018; Asano et al., 2019). Experiments can be performed on robots that would not be practical or ethical if done on human test subjects. Additionally, modifying robotic platforms is potentially faster and cheaper than human observation studies.

Biomimetic robots that are built with artificial muscles provide opportunities to investigate how muscles are controlled to produce desired motions. McKibben style braided pneumatic actuators (BPAs, also called Pneumatic Artificial Muscles or PAMs) are a promising method of actuation because they have low weight, high force/weight ratio, high efficiency, and a force-length curve that is similar to actual muscle []. [2-3 sentences of artificial muscle robots - Asano, Hosoda, Hunt] Combining these artificial muscles with muscle control schemes that have been developed using muscle models in simulation [] can allow for more effective investigations of dynamic interactions with the environment than current physics simulators have to offer. Unfortunately, these artificial muscles don't fully match their biological counterpoints, and there are few tools or design methodologies for BPA attachment locations on robotic systems.

Our previous research has worked to bridge this gap through the development of better models and muscle placement algorithms. We developed a more accurate force-pressure-length model of $\phi 10\,\mathrm{mm}$ Festo BPAs that incorporates changes that arise from different initial lengths (Hunt et al., 2017). We also investigated how the location of muscle attachments affects the torque capabilities of each muscle and compared these capabilities with human data (Bolen and Hunt, 2019). We found that if artificial muscles are placed in the same locations as human muscles, the robot would not be able to achieve the same range of motion or torque that humans achieve. To improve the range of motion and torque produce by the muscles, we developed optimization methods that find attachment locations that can produce a torque curve and range of motion that match human capabilities (Morrow et al., 2020). However, these methods had not been validated on a physical robot body.

Deviation between calculated and measured joint torques could occur through several mechanisms. Festo reports that there can be a 10% deviation from theoretical force due to manufacturing differences ((Festo, 2022)), and it is unclear how well the previous model (Hunt et al., 2017) holds true at high forces. Bending and kinking of the artificial muscle as it wraps around a joint will also reduce the force produced by the muscle. Joint friction can cause a decrease in torque, as can non-rigid elements of the artificial leg. For these reasons we also hypothesize that the experimentally measured torque values will be lower than what is predicted by our theoretical model, and correction factors will need to be incorporated in the modeling system.

This work sets out to fill in these gaps by developing a better model of maximum force produced by $\phi 10\,\mathrm{mm}$ Festo BPAs, and extending this model to $\phi 20\,\mathrm{mm}$ Festo BPAs, which are needed to produce the high torques found about the human knee joint. We then built an isometric knee test stand that enables us to measure the torque about the knee joint at various configurations. Data collected from the test stand is compared with theoretical torque values, and used to develop an improved model that incorporates loses due to compliance. We also demonstrate that the improved attachment locations produced by the optimization method in previous work are able to produce torques that match or exceed human capabilities across a wide range of motion.

2 METHODS AND MATERIALS

2.1 Overview

First, we built a jig to measure artificial muscle force as a function of length and pressure. We tested 10 mm and 20 mm muscles with various initial lengths and at different contraction lengths. This data was used to develop an improved model that better predicts maximum muscle force based on initial muscle length and current muscle length. We then built a jig to test the torque produced by the artificial muscles about a knee joint. With the expectation that measured torque will be less than that predicted by the model, the robot muscle arrangement and knee design were simplified to elucidate the variables that most effect the results. Two joints were used and tested: a simplified pinned knee joint and a biomimetic 1-DoF knee (Steele et al., 2018). Each joint was driven by a single flexor and single extensor muscle. We also varied muscle origin/insertion locations, initial length, diameters, and whether or not they used an artificial tendon. The results from these tests were compared with three virtual models: (1) the human biomechanical model, (2) the conceptual robot model, and (3) the actual robot model.

2.2 Actuator force testing

A test jig was made of 80/20 1515 series extruded aluminum (Fig. XX). Artificial muscles were placed vertically in the jig. The upper end was attached to an Loadstar S shaped load cell. The lower end was attached to an adjustable crossbeam used to change the length of the actuator. Compressed air was supplied through the building at 620 kPa (90 PSI) and measured with an MXPXXXX pressure sensor.

Each BPA l_{rest} was measured as the distance between the hose clamps. This is how Festo defines l_{rest}, although in (Hunt et al., 2017) it was measured to also include end cap length.

We then inflated each BPA to $P_{max} = 620\,\mathrm{kPa}$ and measured ϵ_{max}. The BPAs were then deflated, placed vertically in the test jig made out of 80/20 1515 series extruded aluminum pieces and fixed between two crossmembers. The force sensor was placed between the upper crossmember and the BPA. For $120\,\mathrm{mm}$, $220\,\mathrm{mm}$, $260\,\mathrm{mm}$, $281\,\mathrm{mm}$ and $281\,\mathrm{mm}$ l_{rest}, a Loadstar S Shaped load cell was used instead of the other force sensors previously mentioned. The distance between the crossmembers was adjusted to get different amounts of ϵ^*. The BPAs would then be inflated. BPAs with l_{rest} of $120\,\mathrm{mm}$, $220\,\mathrm{mm}$, $260\,\mathrm{mm}$, $281\,\mathrm{mm}$ and $281\,\mathrm{mm}$ had a lot of P variation, with only 4–5 different values of ϵ^* per BPA. Conversely, BPAs with l_{rest} of $112\,\mathrm{mm}$, $415\,\mathrm{mm}$, $455\,\mathrm{mm}$, $490\,\mathrm{mm}$ and $518\,\mathrm{mm}$ had many different values of ϵ^* recorded, but all values were taken at or near P_{max}. F and P data are collected as described in a previous subsection, above.

2.3 Robot Architecture

Components of the robot leg are the knee joint, femur, tibia, BPAs, BPA end caps, artificial tendon, and attachment brackets (Fig. 1). The artificial bone components are 3D printed using Onyx material on Markforged Onyx One and Mark Two printers. Onyx is a proprietary Markforged material that consists of chopped carbon fiber in nylon. Certain brackets also included carbon fiber layers to increase stiffness. Artificial tendon is made with Shimano bicycle brake cable for $\phi 10\,\mathrm{mm}$ BPAs, and wire rope with the $\phi 20\,\mathrm{mm}$ and $\phi 40\,\mathrm{mm}$ BPAs. When using the brake cable we first apply load to it and induce plastic deformation so that during the test the cable only has elastic deformation.

One uniarticular knee extensor and one uniarticular knee flexor are used to actuate the joint. Each knee knee joint type is tested using $\phi 10\,\mathrm{mm}$ Festo BPAs. Additionally, for the biomimetic knee joint, the biceps femoris short head muscle was mimicked using a $\phi 20\,\mathrm{mm}$ Festo BPA, and the vasti muscles are mimicked

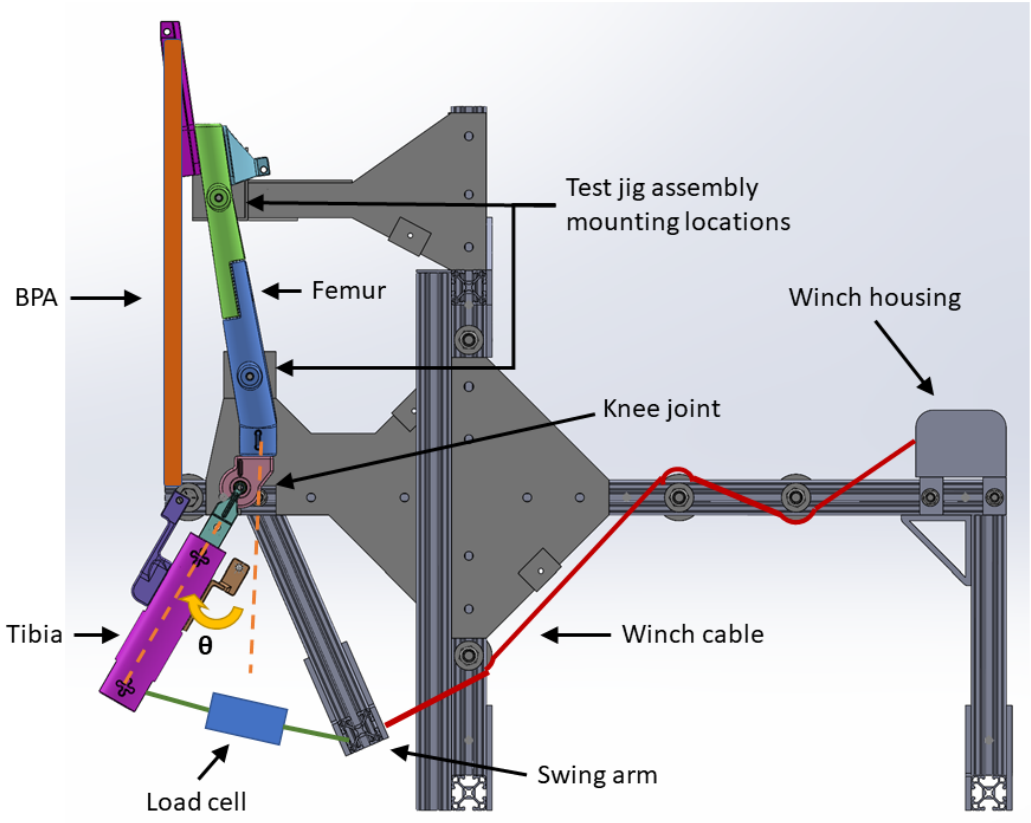

Figure 1. 1-DoF pinned-joint robot knee in the test apparatus with important components labeled. Leg is shown with 30 degrees flexion, i.e. $\theta_k = -30°$

using one $\phi 40\,\mathrm{mm}$ Festo BPA. The artificial muscle is pinned to the muscle origin location, while the other end is either pinned or is free floating and attached to the muscle insertion location via an artificial tendon.

Steele designed the biomimetic robot knee used in this study (Steele et al., 2018, 2017). A 1-DoF joint is achieved by using a four bar linkage mechanism. The intersection point of the crossed links define the knee frame origin and ICR. This allows the joint ICR location in the femur frame (p_k) to translate in the $\hat{x}$ and $\hat{y}$ directions during knee rotation (see Figs. 1 and 2**B**). Having a moving ICR complicates test stand construction. If the joint were of a pinned revolute design, a torque motor could have been used to measure M. Translation as a function of knee angle is also how the human knee behaves.

The leg assembly geometry and dimensions are based off of bones scans of a $6\,ft$ tall ($\sim 1.83\,\mathrm{m}$) person. Each joint is driven by two antagonistic Festo actuators that act as artificial muscles. Both joints have the same location in the femur frame (p_k) at $\theta_k = 0\,\mathrm{deg}$ as the human benchmark model. A test jig constrains the robot to saggital planar motion (Fig. 2). This system has two mounting locations to fix the femur to the frame. To eliminate the effect of gravity on our test results, the robot saggital plane was made parallel with the horizontal plane of the ground.

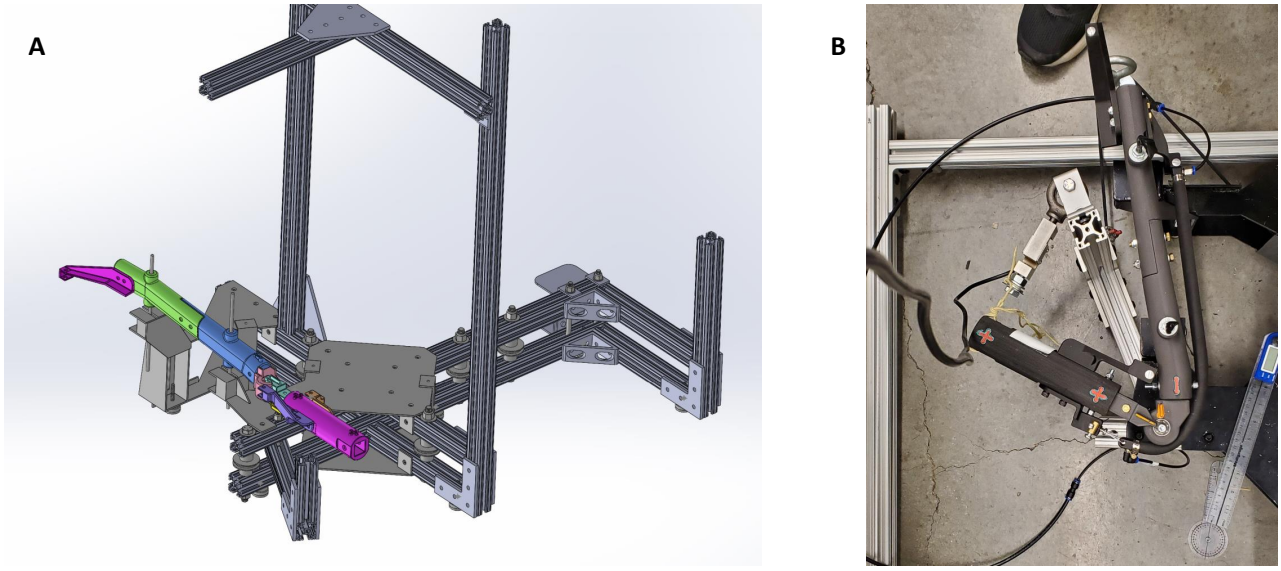

Figure 2. **(A)** CAD solid model assembly of the revolute joint knee in the test stand. **(B)** Picture of robot leg in test jig. Setup shows the pinned knee configured for a test of the extensor BPA. The knee is flexed with $\theta_k = -120°$. The S shaped load cell attaches the tibia to the swing arm and is nearly perpendicular to the tibia in this configuration. Also note the compressed shape of the inflated BPA during this high degree of flexion.

2.4 Moment arm and Torque calculations

2.4.1 Classical mechanics

The goal of this study is to compare measured robot performance to both calculated robot performance and also to what we expected from a human's reported maximum M. The classical mechanics way to calculate torque $\vec{M}$ about the joint is to take the cross product of $\vec{d}$ and $\vec{F}$

$$\vec{M} = \vec{d} \times \vec{F} \tag{1}$$

where distance $\vec{d}$ is from the joint to the force's line of action of represented by $\vec{F}$ The calculations for human muscle F and joint M that we used as a benchmark were from Delp, Hoy, Yamaguchi, Sherman, Millard, and Thelen (Delp et al., 1990; Hoy et al., 1990; Yamaguchi and Zajac, 1989; Sherman et al., 2013; Millard et al., 2013; Thelen, 2003). Reference human values were obtained using the Gait2392 model in the biomechanical modeling software OpenSim (Delp et al., 1990; Seth et al., 2011, 2018). Gait2392 is the anatomical human biomechanical model used for comparison. Fig. 3 shows the human uniarticular knee flexor and extensor muscle actuators.

2.4.2 Moment arm

Moment arm $\vec{r}$ is the shortest $\vec{d}$ to $\vec{F}$. In this study it is calculated using the method specified by Young and colleagues (Young et al., 2019). The moment arm, $r_{\hat{k}}$, about the $\hat{z}$ axis is calculated by:

$$r_{\hat{k}} = \vec{p_{proj,i}} \cdot \frac{\vec{p_f} \times \hat{k}}{\|\vec{p_f} \times \hat{k}\|} \tag{2}$$

$\vec{p_{proj,i}}$ is the free muscle segment projected onto the xy–plane which is normal to the joint axis. $\vec{p_f}$ is the projected muscle segment vector. Moment arm is calculated in the body frame.

Figure 3. View of the human biomechanical model Gait2392 used for comparison. In this test we looked at the uniarticular muscles that attach to the femur and cross the knee, shown as red muscle actuators in the picture.

2.4.3 Wrench

Experimentally determined M is calculated using the wrench.

2.4.4 Hybrid method

The hybrid method is a way of back calculating torque from experimentally measured values.

2.5 Data Collection: Equipment and Procedures

We built a jig to collect knee M measurements at different knee angles (θ_k) over its RoM. The test stand frame is made predominantly out of 80/20 1515 series extruded aluminum components. The knee joint is allowed to rotate while the femur is fixed to the frame. A force sensor has one end connected to the tibia and the other is connected to a swing arm. The swing arm is tied to the winch with $3/16$ inch Kevlar rope from Quality™ Nylon Rope (see Figs. 1 and 2**B**. This rope has a Kevlar core with a polyester jacket and is rated to have a break strength of 1150 lbs.

Force data was collected using one of two different sensors. The first was a MODERN STEP $300\,\mathrm{kg}$ digital crane scale. The second force sensor is a CALT DYLY-103 $100\,\mathrm{kg}$ S shaped load cell. The was load cell was used in conjunction with a HX711 Load Cell Amplifier. P data comes from a Freescale MPX5700 GP $5\,\mathrm{V}$ pressure sensor. Building air supply pressure was controlled with two pressure regulators in series. The first is a Parker model 20R113GC 0-120 psi pressure regulator. The second is a Husky $3/8\ in$. High Performance Air Regulator HDA72200. A Festo VTUG-10-MRCR-S1T-26V20-T516LA-UL-T532S-8K valve manifold VTUG-G was used to deliver air from the pressure regulator to the actuator. This manifold

is comprised of eight two-in-one bidirectional normally closed Festo VUVG-S10-T32C-AZT-M5-1T1L valves.

P and load cell amplifier data are sent to Matlab via an Arduino Uno style Sparkfun BlackBoard C microcontroller. The computers that used Matlab were running either Windows 10 and Windows 11. During phases when the Arduino was collecting F and P data to send to Matlab, the Arduino would also trigger (via Matlab) an Onsemi 2N4401 NPN transistor to make valve manifold open or close the valve. For other data collection the valve was manually opened and closed.

Length measurements were done using a FANUC tape measure. When there was sufficient curvature in the BPA during knee extensor torque tests, a flexible piece of string to was used to mark the axial length, and then the distance was determined with the tape measure. Other times we were able to measure the extensor length using iBayam flexible tape measures.

Angle measurements were taken with either a Medigauge digital electronic goniometer or with MALENOO analog goniometers of 6, 8, or 12 inch lengths. The angle of the knee joint and the angle of the force sensor to a predefined line on the tibia were the angle measurements of interest to us. The latter angle allows us to calculate torque as the force sensor was not always perpendicular with the tibial axis.

2.6 Actuator Force Calculation

Human muscle-actuator F is calculated using the Hill muscle model. Specifically, we relied on the equations as described by Millard (Millard et al., 2013) and used in OpenSim model Gait 2392. The specifics equation and values are detailed in previous work by Bolen and Morrow (Bolen and Hunt, 2019; Morrow et al., 2020).

BPA actuator F in our previous work has been calculated from a FLP relationship derived by Hunt (Hunt et al., 2017). For a given robot configuration and P (in kPa), the scalar force F (in Newtons) for each of the artificial muscles can be determined by solving the equation:

$$P = 254\,\mathrm{kPa} + 1.23\,\frac{\mathrm{kPa}}{\mathrm{N}} \cdot F + 15.6\,\mathrm{kPa} \cdot S + 192\,\mathrm{kPa} \cdot \tan\left(2.03\left(\frac{\epsilon}{-0.331 \times 10^{-3}\,\frac{1}{\mathrm{N}} \cdot F + \epsilon_{max}} - 0.46\right)\right) \quad (3)$$

ϵ is the amount of contraction, and ϵ_{max} is the maximum amount of contraction in a BPA without external load that is inflated to $620\,\mathrm{kPa}$. S is the hysteresis factor of the artificial muscle in which $S = 1$ indicates the muscle is shortening and with $S = -1$ it is lengthening. For isometric contraction, set $S = 0$. An important note for (3) is that the coefficients have been updated with the correct values as the previous version contained typos. We used this corrected version of the equation to create a lookup table for actuator F for a given amount of P and relative strain ϵ^*, defined as

$$\epsilon^* = \frac{\epsilon}{\epsilon_{max}} \quad (4)$$

With this lookup table created it is possible to use a curve fit to develop an equation for F as a function of P and ϵ^*. However, we note here two problems with the BPA characterization in (Hunt et al., 2017).

The first is that this testing was done with a maximum of $111.2\,\mathrm{N}$ applied load, which is only about 20% of the maximum F (F_{max}) specified for the Festo BPA at maximum pressure P_{max} and $\epsilon^* = 0$. Secondly, we observed that F_{max} in the $\phi 10\,\mathrm{mm}$ BPA decreases as l_{rest} decreases. Therefore, we created a test jig apparatus to test F for various l_{rest} of $\phi 10\,\mathrm{mm}$ Festo BPAs at different P values.

3 RESULTS

Results from BPA characterization tests are shown first in Fig. 4. Fig. 4**A** and fig. 4**B** shows a force response resembling an $\arctan$ curve along the l_{rest} dimension and with a more linear response along the P axis. We used a surface fit to find the equation for maximum force in a $\phi 10\,\mathrm{mm}$ BPA as a function of l_{rest} and P, i.e. $F_{max_{10}}(l_{rest}, P)$.

$$F_{max_{10}}(l_{rest}, P) = a1 \cdot P \cdot \arctan\left(a2 \cdot P \cdot (l_{rest} - 0.0075)\right) \tag{5}$$

l_{rest} is offset by $7.5\,\mathrm{mm}$ because solid modeling showed our endcaps contact each other at $l_{rest} = 0.0075\mathrm{mm}$. Therefore $F_{max_{10}}(7.5\,\mathrm{mm}) = 0$ because air would flow in one endcap and out the other (assuming perfect alignment). The curve fitting was done using the Nonlinear Least Squares method and a Least Absolute Residual robustness. $a1 = 0.4848\,\mathrm{N\,kPa^{-1}}$ (0.4848–0.488 with 95% CI) and $a2 = 0.033\,06\,\mathrm{kPa^{-1}\,m^{-1}}$ (0.0325–0.03362 with 95% CI). 5 has an Adjusted $R^2 = 0.9997$ and an RMSE $= 2.749$. Substituting $P_{max} = 620\,\mathrm{kPa}$ into 5 yields the following simplified equation:

$$F_{max_{10}}(l_{rest}) = 301.6\,\mathrm{N} \cdot \arctan\left(20.5\,\mathrm{m^{-1}} \cdot (l_{rest} - 0.0075)\right) \tag{6}$$

Equation 6 is compared with the data in fig. 4**B**. It can be seen that $\lim_{l_{rest}\to\infty} F_{max_{10}} = 473.7\,\mathrm{N}$. Fig. 4**C** shows an attempt at a linear fit for $\epsilon_{max}(l_{rest})$. There was a large amount of variance in the data, with the linear fit giving an adjusted $R^2 = 0.4124$ and an RMSE $= 0.0083$, therefore at this time we cannot say with confidence that there is a linear relationship between maximum strain and l_{rest}.

The next step in BPA characterization we derived an equation for normalized force in the BPA, or $F^* = F/F_{max}$. In previous work we have already used relative strain $\epsilon^* = \epsilon/\epsilon_{max}$ (4), and here we will also introduce relative pressure $P^* = P/P_{max}$. Then we can show that $F^*(\epsilon^*, P^*)$ (Fig. 5). By visualizing the lookup tables discussed above, and the Festo Corporation data sheet, we can see that there appears to be an exponential relationship between ϵ^* and F, and a linear relationship between P and F. A polynomial surface fit also shows an interaction between the linear P and exponential ϵ^* terms. Therefore we fit a surface to the original data using an equation of the form

$$F^*(\epsilon^*, P) = b0 + \exp\left(-b1 \cdot \epsilon^* + b2\right) + P \cdot \exp\left(-b3 \cdot \epsilon^{*2} + b4\right) + b5 \cdot P^* \tag{7}$$

With all the additional data collected on $\phi 10\,\mathrm{mm}$ BPAs with l_{rest} given in fig. 4, we then normalized the force data collected by dividing each BPA's force results by $F_{max_{10}}$ for that BPA. P data was divided by P_{max} This reduced much of the variance in the data, as shown in fig. 5, which qualitatively pointed towards using a surface fit as the right approach for F^*. Using ϵ^* and P^*, it was possible to reduce the amount of coefficients in Eq. 7 from six to only two. The equation for normalized force is

$$F^*_{10}(\epsilon^*, P^*) = -1 + \exp\left(-c1 \cdot \epsilon^*\right) + P^* \cdot \exp\left(-c2 \cdot \epsilon^{*2}\right) \tag{8}$$

with $c1 = 1.7$ (1.692–1.708 with 95% CI) and $c2 = 0.2$ (0.1968–0.2029 with 95% CI). This surface fit was done using Nonlinear Least Squares method and Least Absolute Residuals robustness. Additional data from separate tests using the l_{rest} values of $120\,\mathrm{mm}$, $220\,\mathrm{mm}$, $260\,\mathrm{mm}$, $281\,\mathrm{mm}$ and $281\,\mathrm{mm}$ were used for validation. Eq. 8 has an Adjusted $R^2 = 0.9998$, SSE $= 0.007833$, and an RMSE $= 0.0057$. Validation

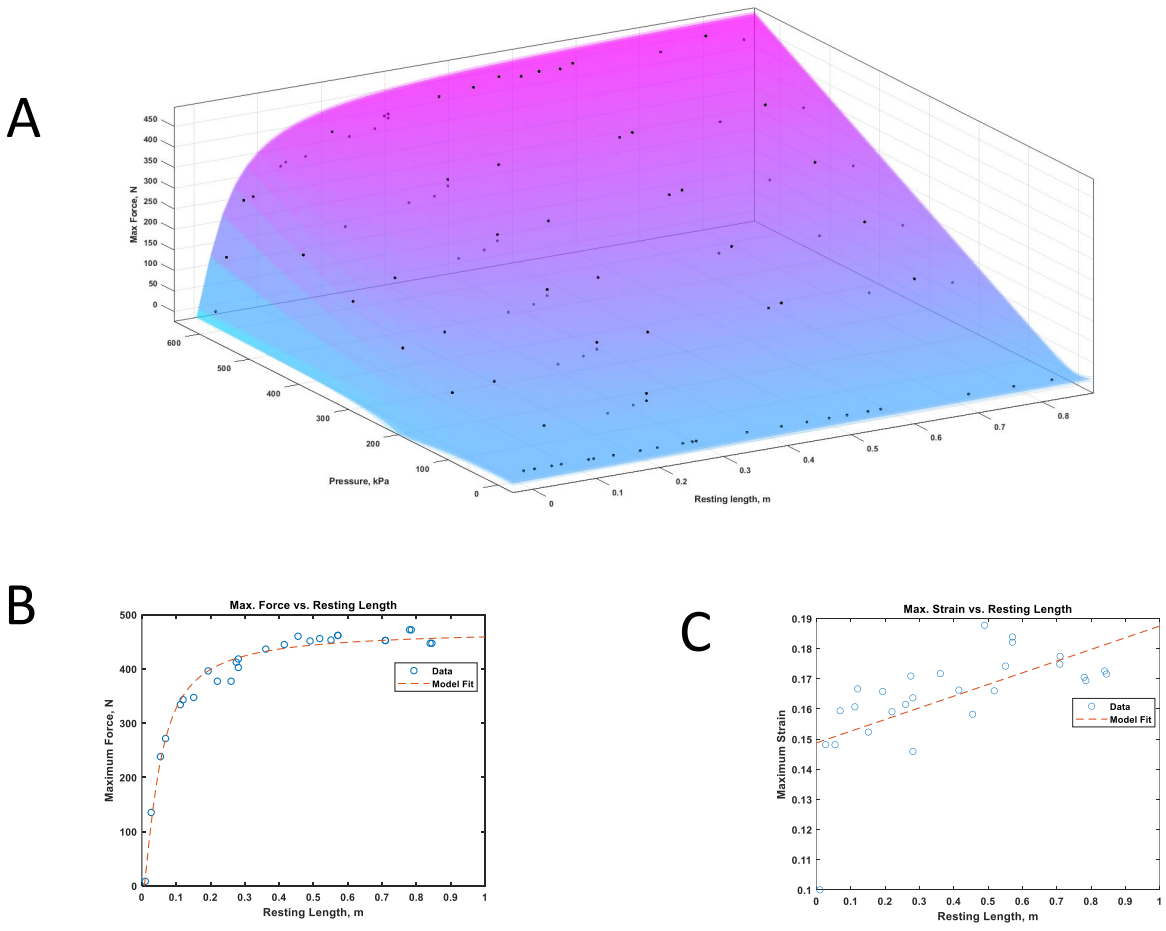

Figure 4. Results for finding the relationship between l_{rest} and $F_{max_{10}}$, ϵ_{max}. **(A)** Surface fit for $F_{max_{10}}(l_{rest}, P)$. **(B)** $F_{max_{10}}$ versus l_{rest} at $P_{max} = 620\,\text{kPa}$. **(C)** ϵ_{max} versus l_{rest} at $P_{max} = 620\,\text{kPa}$. No conclusive relationship between ϵ_{max} and l_{rest} could be deduced from this experiment.

SSE $= 0.482595$ and RMSE $= 0.044292$. Combining Eq. 8 and Eq. 6 will now allow researchers to determine the force F in a BPA given l_{rest}, P^*, and ϵ^*.

$$F(\epsilon^*, P^*, l_{rest}) = F^*(\epsilon^*, P^*) \cdot F_{max}(l_{rest}) \tag{9}$$

Force functions for $\phi 20\,\text{mm}$ and $\phi 40\,\text{mm}$ BPAs were also derived. F tests were not performed on these BPA sizes. Instead, values of $F_{max_{20}} = 1500\,\text{N}$, $F_{max_{40}} = 6000\,\text{N}$, $\epsilon_{max} = 25\%$, and $P_{max} = 600\,\text{kPa}$, provided by Festo Corporation (Festo, 2022) were used. The normalized force equation for the $\phi 20\,\text{mm}$ BPA is

$$F^*_{20}(\epsilon^*, P^*) = b0 + \exp\left(-b1 \cdot \epsilon^* + b2\right) + P \cdot \exp\left(-b3 \cdot \epsilon^{*2} + b4\right) - b4 \cdot P^* \tag{10}$$

From this equation, it can be seen that the coefficient $b4 = -b5$ appears twice. Eq. 10 has an Adjusted $R^2 = 0.9985$, SSE $= 0.0125$, and an RMSE $= 0.0154$. The $\phi 40\,\text{mm}$ BPA fit equation is

$$F^*_{40}(\epsilon^*, P^*) = b0 + \exp(-b1 \cdot \epsilon^* + b2) + P \cdot \exp(-b3 \cdot \epsilon^* + b4) + b5 \cdot P^* \quad (11)$$

It can be seen that 11 is similar to the structure of Eqns. 7 and 10, but with an ϵ^* term in the second exponential instead of ϵ^{*2}. Eq. 11 has an Adjusted $R^2 = 0.9999$, SSE $= 8.614 \times 10^{-4}$, and an RMSE $= 0.0040$.

The new method of calculating $10\,\mathrm{mm}$ BPA force is used to calculate maximum M for the various configurations. Starting with the simplest case, we examine BPAs of l_{rest} $45.7\,\mathrm{cm}$ and $48.5\,\mathrm{cm}$ on the pinned knee used for knee flexion (fig. 6). Fig. 6**A** shows measured torque as blue diamonds and expected (theoretical) torque as a magenta line. Experimentally measured values of BPA length, P, and moment arm were used with Eq. 9 to back calculate torque values. It was determined that a major part of the discrepancy in measured versus expected torque values was due to differences in measured versus expected ϵ^* values (Fig. 6**B**). After running an optimization algorithm to change the length of the end cap fitting, Fig. 6**C** shows improved results. The results of the optimization were validated with the $45.7\,\mathrm{cm}$ M values (fig. 6**D**). The fitting length in the algorithm is changed from $25.4\,\mathrm{mm}$ to $35.2\,\mathrm{mm}$. The optimization yielded an SSE $= 554.6$ and the validation returned a SSE $= 315.3$ with a RMSE $= 2.96$.

Pinned knee extensor results using $\phi 10\,\mathrm{mm}$ Festo BPAs of l_{rest} $41.5\,\mathrm{cm}$, $45.7\,\mathrm{cm}$ and $48.5\,\mathrm{cm}$ are shown in Fig. 7. Measured torque was slightly higher than expected in the $48\,\mathrm{cm}$ BPA whereas it was slightly lower than expected in the $45.7\,\mathrm{cm}$ BPA. The $41.5\,\mathrm{cm}$ BPA was used in two configurations: with and without an artificial tendon. Previous optimization wasn't used with these results.

Why the discrepancy between the results? The first two seem acceptable, but not perfect. The shorter the l_{rest}, the more the results are less than expected. Comparing measured values of l_m and ϵ^* to theoretical shows a close correlation, but would increase torque for the first two and decrease for the second. The BPA w/ artificial tendon shows a discrepancy, so maybe the tendon length was measured incorrectly? Well, maybe looking at Fig. 2**B** again can shed some insight? It would be possible to bring it into the Matlab image acquisition toolbox to analyze lengths. If I can also show somehow that the shorter lengths tend to kink then that would also let us create a nonlinear torque correction factor along the lines of $M_{\hat{k}} = r\vec{k} \times (F - cf \cdot F \cdot \theta_k)$. Improved solid model might also help?

Fig. 8 shows the results optimized flexor calculation method in the biomimetic knee for a $\phi 10\,\mathrm{mm}$ $l_{rest} = 41.5cm$ BPA with a $12\,\mathrm{mm}$ artificial tendon made out of Shimano bicycle brake cable. Comparing the previous method of calculating torque to the measured torque results in an SSE $= 287.3$ and an RMSE $= 5.36$. The optimized torque calculation fits much better with a SSE $= 1.282$ and a RMSE $= 0.358$. Experimentally measured values were again used to back calculate torque, although we note that moment arm $r_{\hat{k}}$ was measured from knee ICR, not p_k, and that experimentally measuring $r_{\hat{k}}$ is less precise ($\pm 5\,\mathrm{mm}$) in the biomimetic knee versus the pinned knee.

We obtained results for M in 9 using the biomimetic knee with a $\phi 10\,\mathrm{mm}$ BPA in the extensor configuration. The torque values differ a lot from those we expected. Looking at 9**B** it can be observed that the length is very close to what we expected, but 9**C**. However, again we note that moment arm by hand is measured to the ICR, and using this value would mean we would expect even high torque than what was observed. Fig.10 shows the difficulty of modeling something that passes through the femoral condyles.

Opensim comparison. Full size BPAs in biomimetic knee assembly results. Fig 11 shows the 40mm BPA in the extensor configuration. Fig. **??**

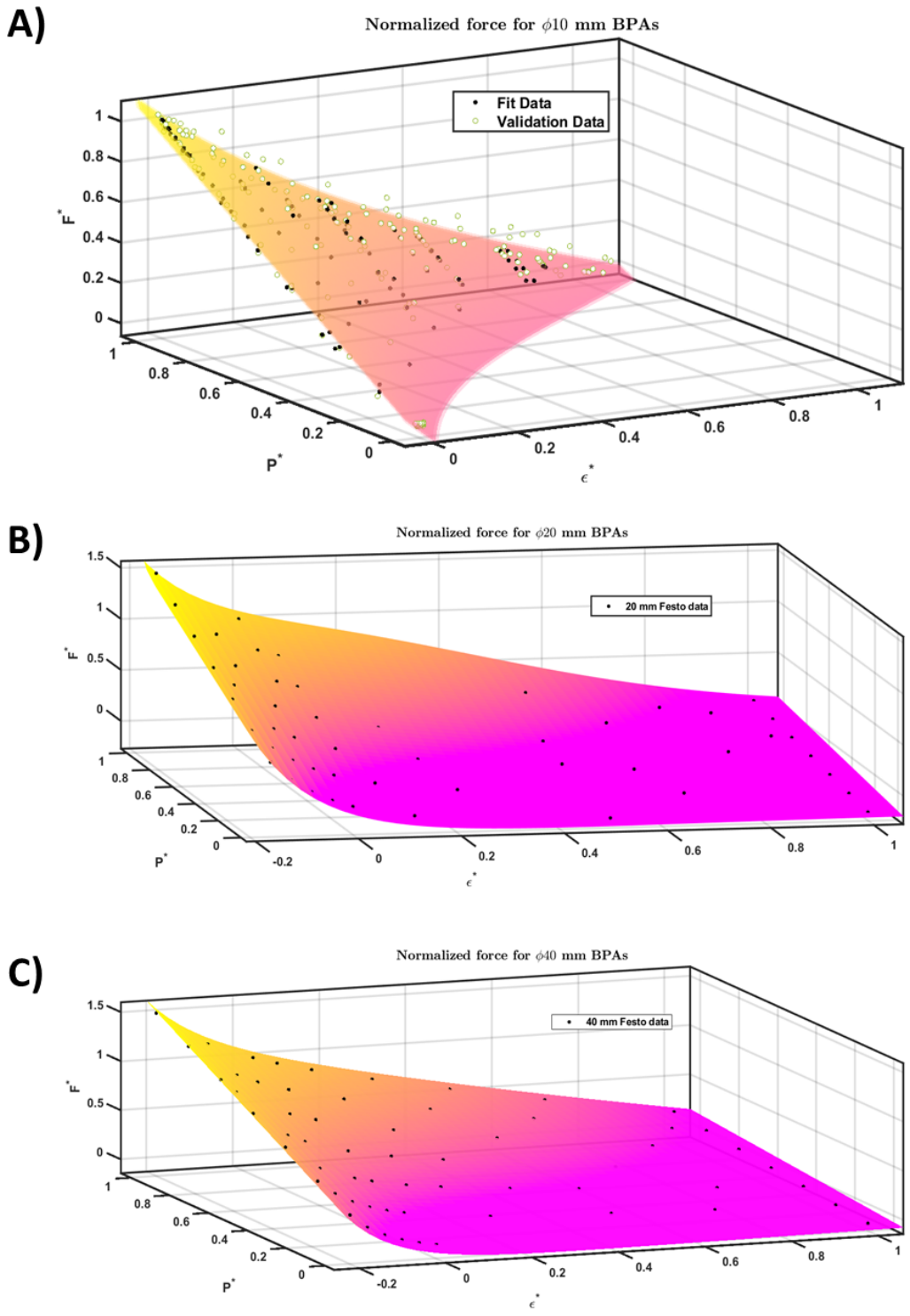

Figure 5. Surface fit for $F^*(\epsilon^*, P^*)$ with (95% CI shown). Black circles represent fit data. **(A)**Fit data for $\phi 10\,\mathrm{mm}$ Festo BPA. Validation data is the green circles. **(B)**Fit data for $\phi 20\,\mathrm{mm}$ Festo BPAs. **(C)**Fit data for $\phi 40\,\mathrm{mm}$ Festo BPAs.

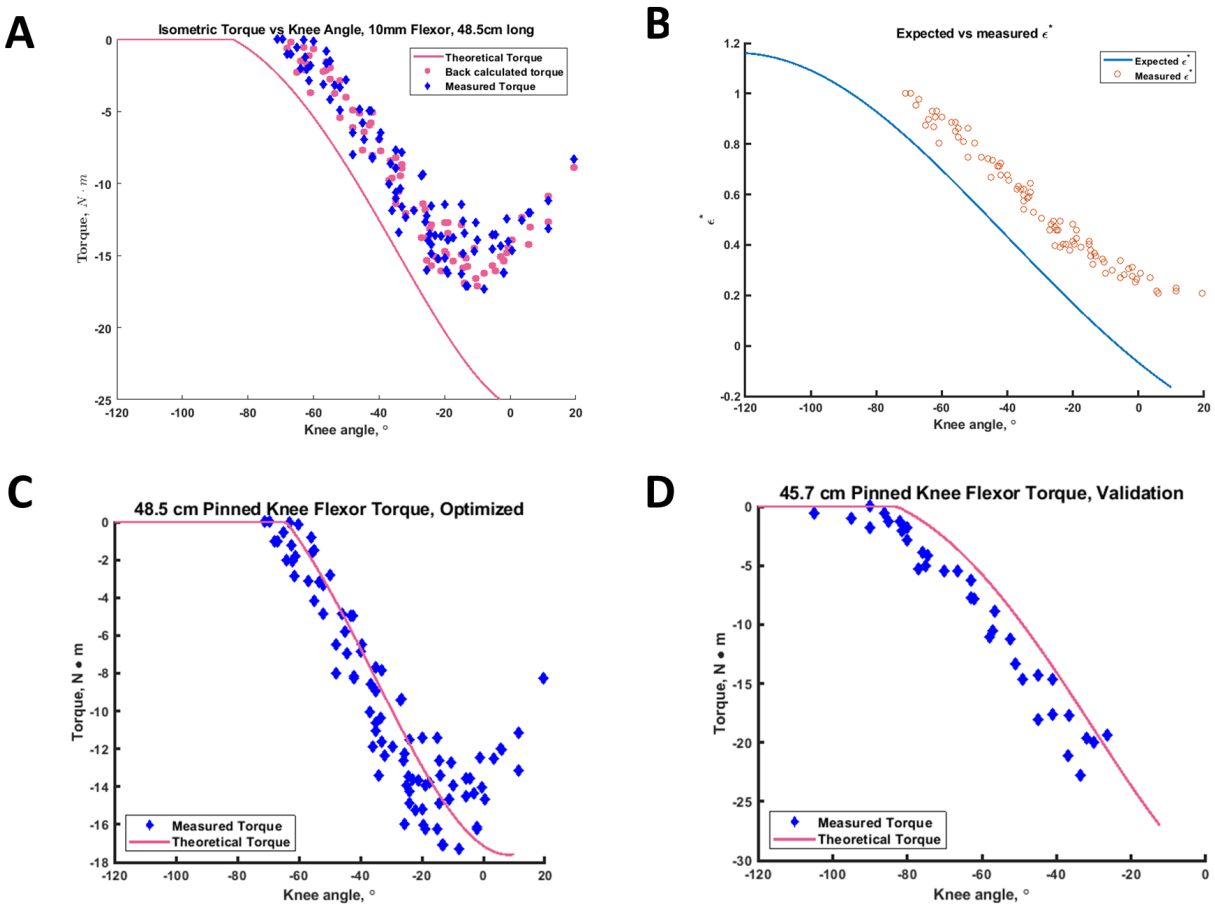

Figure 6. Results for the pinned knee using flexor BPAs. **(A)** Theoretical, measured, and back calculated torque for the $48.5\,\mathrm{cm}$ BPA. **(B)** comparison of measured versus expected ϵ^* for the $48.5\,\mathrm{cm}$ BPA. **(C)** Theoretical and measured torque for the $48.5\,\mathrm{cm}$ BPA using an optimized fitting length of $35.2\,\mathrm{mm}$. **(D)** Theoretical and measured torque for the $45.7\,\mathrm{cm}$ BPA using an optimized fitting length of $35.2\,\mathrm{mm}$

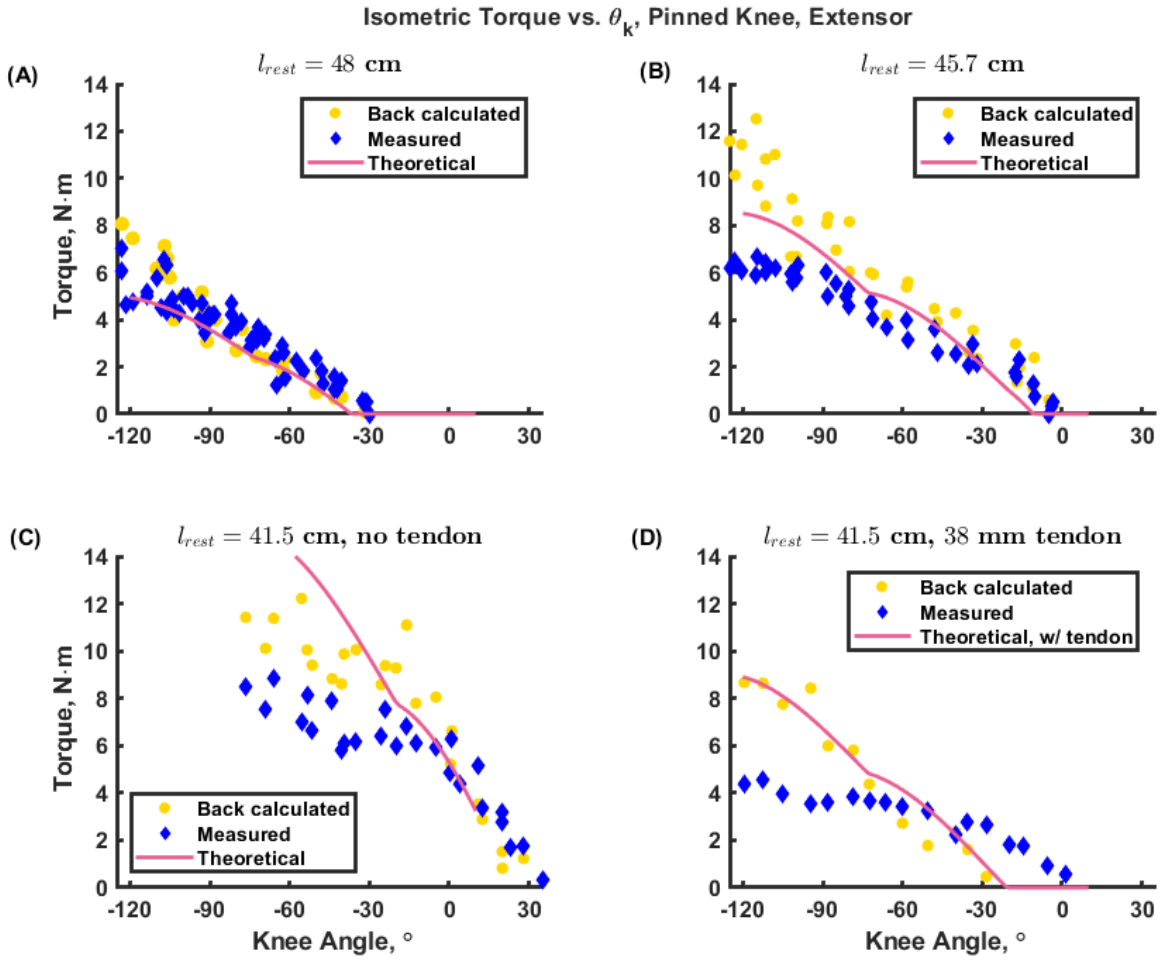

Figure 7. Pinned knee M with the extensor BPA for lengths, **(a)** 48.5 cm, **(A)** 45.5 cm, **(c)** 41.5 cm, and **(D)** 41.5 cm with a 22 mm tendon

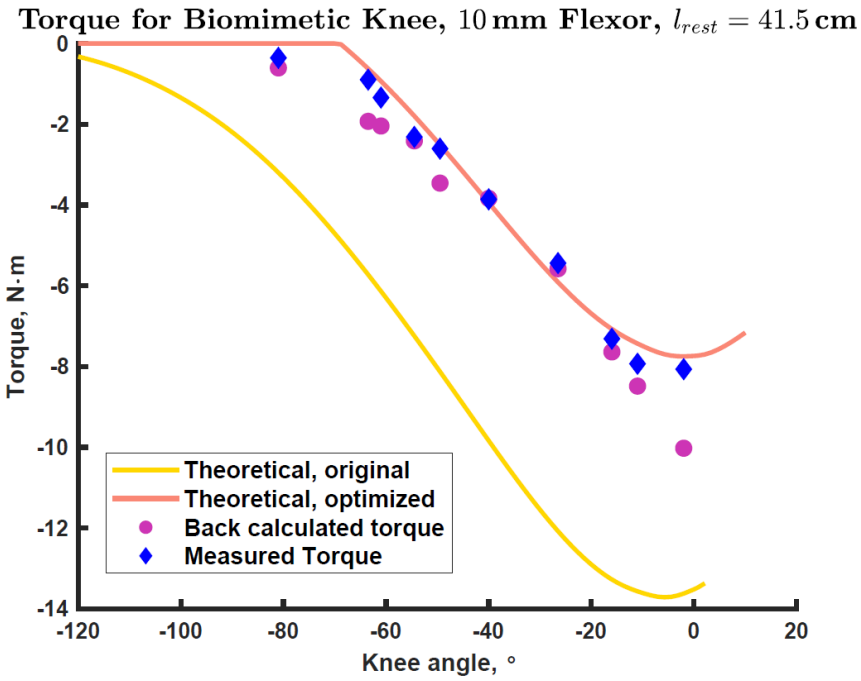

Figure 8. Biomimetic knee M for a $\phi 10\,\mathrm{mm}$ $l_{rest} = 41.5cm$ flexor BPA with a $12\,\mathrm{mm}$ artificial tendon. Blue diamond shows the measured torque values. Light orange line shows the theoretical torque expected using the updated actuator F equation and the optimized fitting length. The yellow line shows the theoretical torque expected using without the optimized fitting length. Magenta circles are torque values back calculated from experimentally measured values of l_m, P, and $r_{\hat{k}}$ (using measurements from knee ICR not p_k).

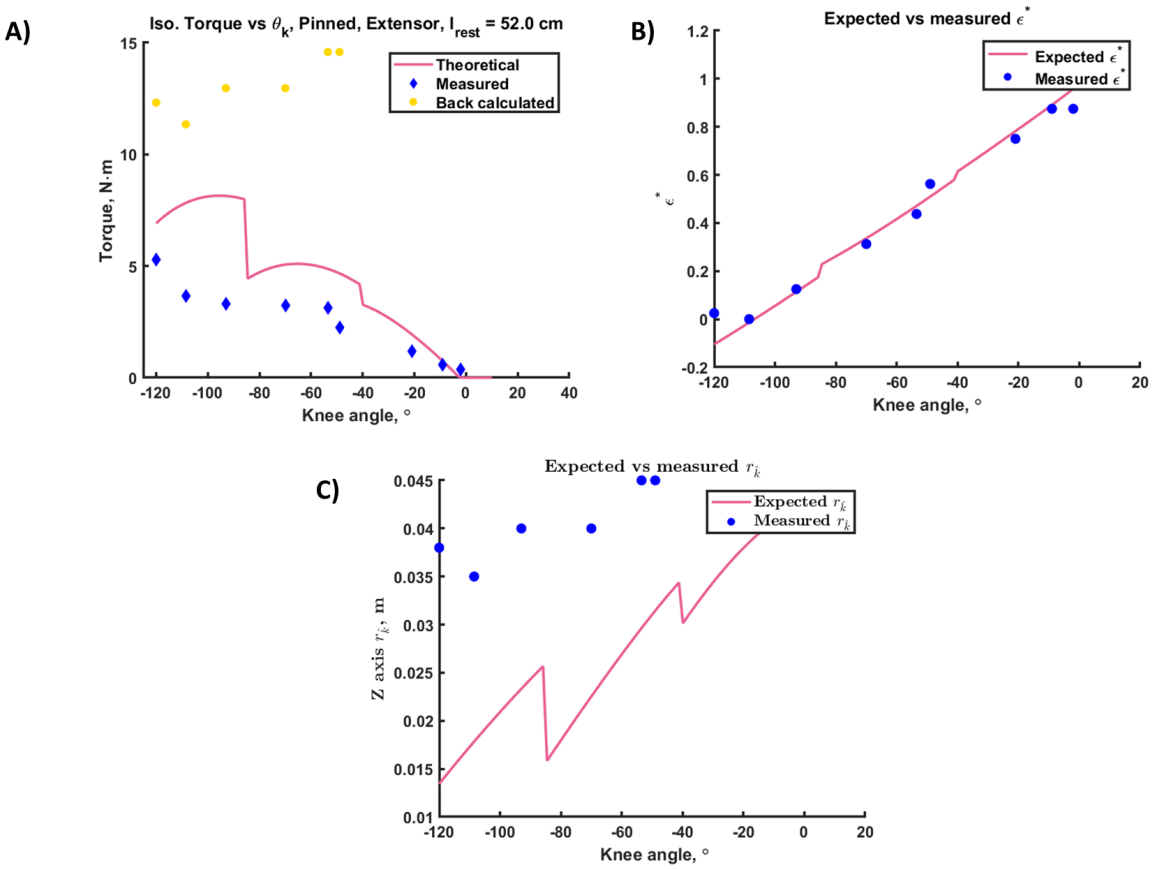

Figure 9. Measured versus expected results using a $\phi 10\,\mathrm{mm}$, $l_{rest} = 51.8\,\mathrm{cm}$ extensor BPA on the biomimetic knee. **A** M. **B** Relative Strain. **C** moment arm.

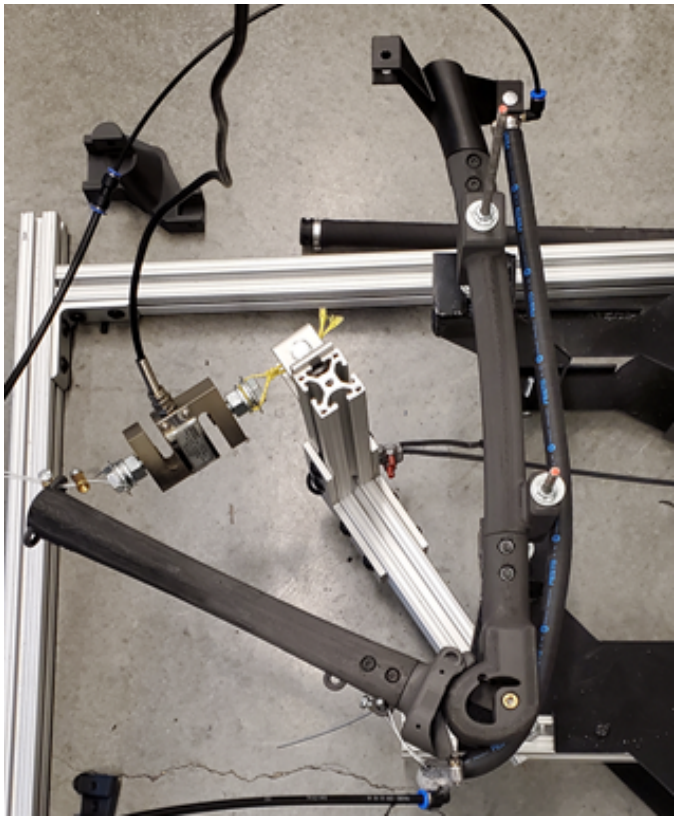

Figure 10. A configuration that is particularly hard to model.

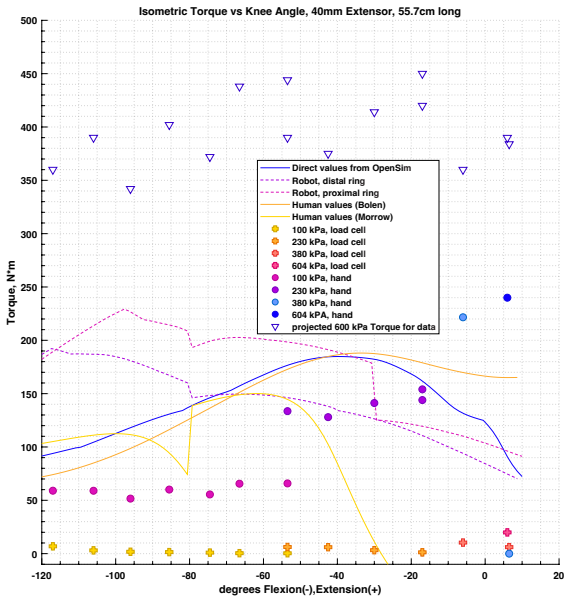

Figure 11. Comparison of M for theoretical BPA values with the humanoid knee, human muscle calculations using our method, and human muscle values as provided by OpenSim. Configurations listed are for **(A)** flexor and **(B)** extensor muscles. Note the major discrepancies between the our human value and OpenSim's, which calls into question the accuracy of our calculations.

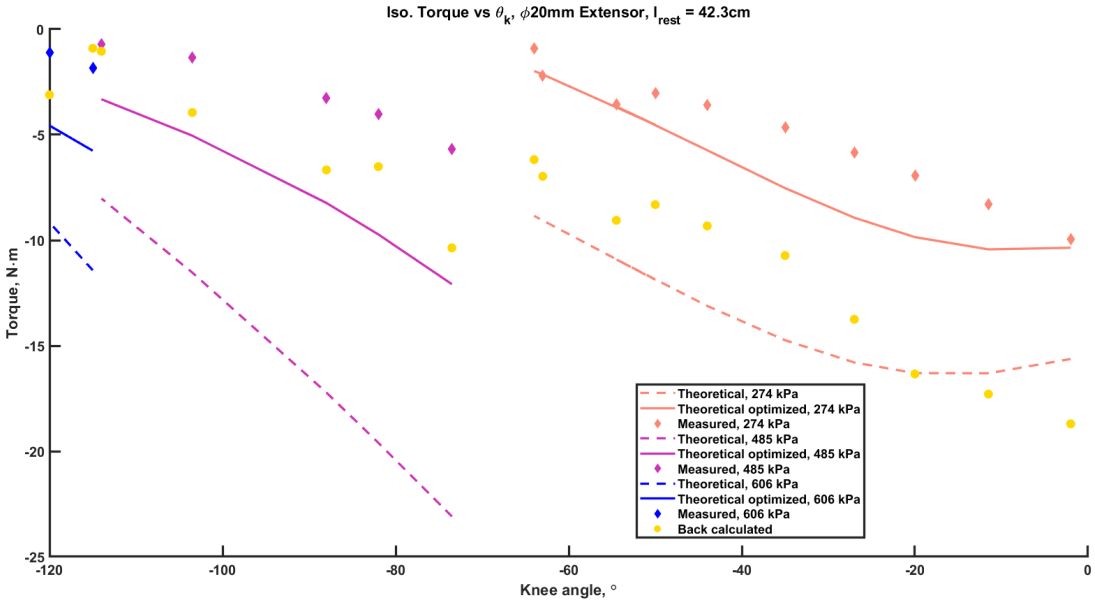

Figure 12. Comparison of measured and theoretical M for the $\phi 20\,\mathrm{mm}$ BPA in flexor configuration. Diamonds represent measured torque values. Dashed lines represent theoretical torque with old fitting length, solid line is the theoretical torque with the optimized fitting length from the previous section. Yellow circles represent values expected from back calculating with BPA length and P known.

4 DISCUSSION

The analysis in this study has allowed us to create novel equations for calculating F in BPAs of $\phi 10\,\mathrm{mm}$(Eqs. 6,8).

There certainly are many factors that affect the M results. Compliance in testing system, flexibility of brackets, imperfect modeling, variation in individual BPAs, etc.

Simplifying the model and testing it allowed us to see how we were deficient in our previous analysis. The isometric system is not rigid. There is compliance in the winch cable, tendons, bending brackets. The modeling of BPA paths is also just an estimate.

Curving BPA during high angles of knee flexion show the BPA being stretched and compressed. It is known that the axial stress in a pressure vessel is

$$\sigma_{\hat{z}} = \frac{F}{A} = \frac{Pd^2}{(d+2t)^2 - d^2} \tag{12}$$

Where $\sigma_{\hat{z}}$ is the axial stress, F is Force, A is area, P is the internal pressure, t is the wall thickness, and d is the mean diameter ($O.D. - t$). In thin wall pressure vessels 12 can be reduced to

$$\sigma_{\hat{z}} = \frac{Pd}{4t} \tag{13}$$

RESOURCE IDENTIFICATION INITIATIVE

- MATLAB (RRID:SCR_001622)
- OpenSim (RRID SCR_002683)
- Arduino UNO (RRID:SCR_017284)

CONFLICT OF INTEREST STATEMENT

The authors declare that the research was conducted in the absence of any commercial or financial relationships that could be construed as a potential conflict of interest.

AUTHOR CONTRIBUTIONS

BB, CM, and AH contributed to conception and design of the study. BB and CM wrote the code to calculate theoretical robot Ms. Figures were created by BB. BB, LB, and LP wrote code for data collection and analysis. BB and LP collected the data. BB performed the statistical analysis and organized the database. BB wrote the first draft of the manuscript. BB, LB, and AH wrote sections of the manuscript. All authors read the manuscript, contributed to its revision, and approved the submitted version.

FUNDING

Research for this article was funded by the Department of Mechanical and Materials Engineering at Portland State University, the National Science Foundation (NSF) grant for NeuroNex: Communication, Coordination, and Control in Systems (C3NS) 2015317 and NSF grant 1943483.

ACKNOWLEDGMENTS

The authors would like to acknowledge the contribution of Alex Steele, who designed the initial biomimetic 4-bar knee linkage we used for the test. He gave us solid models, built a 3D prototype, and let us break said prototype. His prompt and thoughtful responses to our questions about the previous design was very much appreciated. The authors would also like to thank Jasmine Bradley for her help reworking the figures in the results section. As a visual designer, her contributions improved the aesthetic quality of the images. She also helped us choose colors that ensured data accessibility for people with color blindness.

SUPPLEMENTAL DATA

Supplemental Data includes figures for the test setup.

DATA AVAILABILITY STATEMENT

The data sets are available from the authors upon reasonable request.

REFERENCES

Asano, Y., Okada, K., and Inaba, M. (2019). Musculoskeletal design, control, and application of human mimetic humanoid Kenshiro. *Bioinspiration & Biomimetics* 14, 036011. doi:10.1088/1748-3190/ab03fc

Bolen, B. P. and Hunt, A. J. (2019). Determination of Artificial Muscle Placement for Biomimetic Humanoid Robot Legs. In *Biomimetic and Biohybrid Systems*, eds. U. Martinez-Hernandez, V. Vouloutsi, A. Mura, M. Mangan, M. Asada, T. J. Prescott, and P. F. Verschure (Cham: Springer International Publishing), vol. 11556. 15–26. doi:10.1007/978-3-030-24741-6_2

Delp, S., Loan, J., Hoy, M., Zajac, F., Topp, E., and Rosen, J. (1990). An interactive graphics-based model of the lower extremity to study orthopaedic surgical procedures. *IEEE Transactions on Biomedical Engineering* 37, 757–767. doi:10.1109/10.102791

[Dataset] Festo (2022). Festo Fluidic Muscle DMSP

Hoy, M., Zajac, F., and Gordon, M. (1990). A musculoskeletal model of the human lower extremity: the effect of muscle, tendon, and moment arm on the moment-angle relationship of musculotendon actuators at the hip, knee, and ankle. *Journal of Biomechanics* 23, 157–169

Hunt, A., Graber-Tilton, A., and Quinn, R. (2017). Modeling length effects of braided pneumatic actuators. In *IDETC/CIE 2017* (Cleveland, OH: ASME)

Millard, M., Uchida, T., Seth, A., and Delp, S. L. (2013). Flexing Computational Muscle: Modeling and Simulation of Musculotendon Dynamics. *Journal of Biomechanical Engineering* 135, 021005. doi:10.1115/1.4023390

Morrow, C., Bolen, B., and Hunt, A. (2020). Optimization of Artificial Muscle Placements for a Humanoid Bipedal Robot. In *Biomimetic and Biohybrid Systems*

Seth, A., Hicks, J. L., Uchida, T. K., Habib, A., Dembia, C. L., Dunne, J. J., et al. (2018). OpenSim: Simulating musculoskeletal dynamics and neuromuscular control to study human and animal movement. *PLOS Computational Biology* 14, e1006223. doi:10.1371/journal.pcbi.1006223

[Dataset] Seth, A., Sherman, M., Reinbolt, J. A., and Delp, S. L. (2011). OpenSim: a musculoskeletal modeling and simulation framework for in silico investigations and exchange.

Sherman, M. A., Seth, A., and Delp, S. L. (2013). What is a Moment Arm? Calculating Muscle Effectiveness in Biomechanical Models Using Generalized Coordinates. In *Volume 7B: 9th International Conference on Multibody Systems, Nonlinear Dynamics, and Control* (Portland, Oregon, USA: American Society of Mechanical Engineers), V07BT10A052. doi:10.1115/DETC2013-13633

Shin, H., Ikemoto, S., and Hosoda, K. (2018). Constructive understanding and reproduction of functions of gluteus medius by using a musculoskeletal walking robot. *Advanced Robotics* 32, 202–214. doi:10.1080/01691864.2018.1434015. Publisher: Taylor & Francis

Steele, A., Hunt, A., and Etoundi, A. (2018). Biomimetic Knee Design to Improve Joint Torque and Life for Bipedal Robotics (Bristol, UK)

Steele, A. G., Hunt, A., and Etoundi, A. C. (2017). Development of a Bio-inspired Knee Joint Mechanism for a Bipedal Robot. In *Biomimetic and Biohybrid Systems* (Springer, Cham), Lecture Notes in Computer Science, 418–427. doi:10.1007/978-3-319-63537-8_35

Thelen, D. G. (2003). Adjustment of Muscle Mechanics Model Parameters to Simulate Dynamic Contractions in Older Adults. *Journal of Biomechanical Engineering* 125, 70–77. doi:10.1115/1.1531112

Yamaguchi, G. T. and Zajac, F. E. (1989). A planar model of the knee joint to characterize the knee extensor mechanism. *Journal of Biomechanics* 22, 1–10. doi:10.1016/0021-9290(89)90179-6

Young, F., Rode, C., Hunt, A., and Quinn, R. (2019). Analyzing Moment Arm Profiles in a Full-Muscle Rat Hindlimb Model. *Biomimetics* 4, 10. doi:10.3390/biomimetics4010010

FIGURES

TABLES

Table 1. Equations for BPA F with fit and coefficient values

Eq.	Model			Validation		Coefficient	CI (95%)
	Adj. R^2	SSE	RMSE	SSE	RMSE		
5	0.9997	733.2	2.749	–	–	a1 = $0.4864\,\mathrm{N\,kPa^{-1}}$	(0.4848, 0.488)
						a2 = $0.033\,\mathrm{kPa^{-1}\,m^{-1}}$	(0.0325, 0.0336)
6	0.982	5941	14.83	–	–	a1 = $301.6\,\mathrm{N}$	(300.6, 302.6)
						a2 = $20.5\,\mathrm{m^{-1}}$	(20.15, 20.83)
8	0.9998	0.007833	0.006	0.4826	0.0443	c1 = 1.7	(1.692, 1.708)
						c2 = 0.2	(0.197, 0.203)
10	0.9985	0.0125	0.015	–	–	b0 = -0.1881	(-0.2005,-0.1757)
						b1 = 7.965	(7.533, 8.396)
						b2 = -1.677	(-1.755, -1.599)
						b3 = 2.036	(1.733, 2.339)
						b4 = -0.1518	(0.1033, 0.2004)
11	0.9999	$8.614 * 10^-4$	0.004	–	–	b0 = -0.06974	(-0.07298, -0.06651)
						b1 = 8.547	(8.365, 8.728)
						b2 = -2.628	(-2.67, -2.586)
						b3 = 0.2854	(0.2449, 0.3259)
						b4 = 1.148	(1.024, 1.272)
						b5 = -2.128	(-2.519, -1.737)